2021 The 21st International Conference on Control, Automation and Systems (ICCAS 2021)
Ramada Plaza Hotel, Jeju, Korea, Oct. 12∼15, 2021

Performance Comparison between EKF and UKF in GPS/INS Low Observability Conditions

Kyunghyun Ryu[1], Jiseock Kang[2], and Dongjun Lee[2*]

[1]Department of Mechanical and Aerospace Engineering, Seoul National University,
Seoul, 08826, Korea (tomryou@snu.ac.kr)
[2]Department of Mechanical Engineering, Seoul National University,
Seoul, 08826, Korea (jskang0894, djlee@snu.ac.kr)
* Corresponding author

Abstract: For the UAV localization problem, GPS-IMU-based sensor fusion is widely used. In such combination, GPS could correct IMU drift error and IMU could compensate for a low sampling rate of GPS. However, it is known that the GPS-IMU system becomes unobservable for a certain type of maneuver, e.g. hovering as the simplest instance. This paper presents a comparison of two variations of Kalman filter, extended Kalman filter (EKF) and unscented Kalman filter (UKF) for unmanned aerial vehicle (UAV) localization problem in such low observability maneuver. Observability analysis and simulation are conducted on various maneuvers including constant attitude motions and orbit motion. This comparison could help the localization algorithm decision in the development of the UAV system.

Keywords: Global positioning system (GPS), GPS/INS, Inertial navigation, Sensor fusion, Observability, Kalman filter

1. INTRODUCTION

1.1 Background and Motivation

There has been emerging interest in the usage of autonomous unmanned aerial vehicles (UAVs) in the past decade. One important component of autonomous UAV is state estimation, which is an algorithm to provide UAV's current state in real-time by means of sensor fusion.

While several sensing modalities can be employed for UAV state estimation, for example, a vision [1] or a LiDAR [2], the most common selection for outdoor drone flight is an IMU and a GPS. By measuring body acceleration and body angular velocity, the IMU provides the vehicle's orientation and proper body acceleration (i.e., gravity-compensated body acceleration). However, since using only an IMU arises an unobservability to the position and velocity, additional position information is measured by the GPS.

One important notice here is that some states still might not be observable depending on the motion, even when both IMU and GPS are employed. For instance, if the vehicle does not experience any movement, the vehicle's gyro bias in the yaw direction becomes unobservable. More generally, Hong et al., in their work in 2005 [3], showed that the component of gyro bias in the direction of the specific force is unobservable.

Meanwhile, to fuse IMU and GPS, the standard approach is to use optimal sensor fusion methods. The most popular algorithms include extended Kalman filter (EKF) and unscented Kalman filter (UKF). In the EKF, one linearizes the given system and applies a Kalman filter, and in the UKF, one takes sigma points and applies an unscented transform, then applies a Kalman filter. UKF is known to have superior performance than EKF [4] [5].

After the proposal of UKF, its performance evaluation compared to the EKF in GPS-IMU-based sensor fusion has been shown by several authors [6][7]. Their consideration is mainly focused on realistic flight data, where the data has been online recorded in real-world hardware.

Such comparison might give general intuition about the performance of each algorithm. However, due to the cost of the experiment, it is hard to capture the *boundary case behavior* of the algorithm using a real-flight dataset. As mentioned above, there does exist a set of motions to increase an unobservability measure of a GPS-IMU system.

In this paper, we compare the performance gap between EKF and UKF in the above-mentioned low observability motion. Since there exist multiple types of motion to occur the unobservability, and there is no known method to extract all such motion, we restrict our scope to investigate the case of a special subset of motion, namely constant attitude motion and orbit motion. The former is important since many motions in drone flight can be approximated to it, and the latter is important because it is used as a motion primitive in many UAV mission planners.

Since UKF requires more implementation effort than EKF, our comparison might help the decision for the UAV system developers, to choose the algorithm for their state estimation module.

1.2 Contribution

Our contribution can be summarized as follows.

1. We investigate the performance gap between EKF and UKF in the boundary case of the input motion, where the system has an unobservable space in the state.
2. We provide an identification of an important subset of the unobservable motion. (i.e., constant attitude motion and orbit motion). Despite our analysis is mainly replication of the work in Hong 2005 [3] and Rhee 2004 [8],

we gave a minor extension considering the constant attitude case. Also, we provide a comprehensive review of the main points of their analysis.

2. PRELIMINARY

2.1 Extended Kalman Filter

Consider a nonlinear discrete function and discrete measurement

$$x_k = f(x_{k-1}, u_{k-1}) + w_{k-1} \tag{1}$$
$$y_k = h(x_k) + v_k \tag{2}$$

x_k represent the state of the system, u_k denotes the known input, and y_k is the observed signal. w_k and v_k are system noise and measurement noise.

In the prediction stage, we can predict the estimates of state vector $\hat{x}$ with nonlinear function f. We denote predicted values with superscript $-$. P denotes state covariance matrix and it is predicted with linearized state transition matrix F and system noise covariance Q_k. In this paper, the prediction stage is conducted with high-frequency IMU data

$$\hat{x}^- = f(\hat{x}_{k-1}, u_{k-1}) \tag{3}$$
$$P_k^- = F_{k-1} P_{k-1} F_{k-1}^T + Q_k \tag{4}$$
$$F_{k-1} = \frac{\partial f}{\partial x}|_{\hat{x}_{k-1}, u_{k-1}} \tag{5}$$

In the update stage, the filter correction is performed with given GPS data. Kalman gain matrix K_k is obtained by minimizing the mean square state error. The state covariance matrix is updated with Kalman gain matrix K_k and linearized measurement matrix H_k. V_k is the covariance of measurement noise. The equations are given as follows

$$H_k = \frac{\partial h}{\partial x_k}|_{\hat{x}_k} \tag{6}$$
$$K_k = P_k^- H_k^T (H_k P_k^- H_k^T + V_k)^{-1} \tag{7}$$
$$\hat{x}_k = \hat{x}_{k-1} + K_k(y_k - h(\hat{x}_k)) \tag{8}$$
$$P_k = (I - K_k H_k) P_k^- \tag{9}$$

2.2 Unscented Kalman Filter

In the unscented Kalman filter, from the estimated state vector $\hat{x}$, sigma points are calculated as follows

$$X_{k-1} = [\hat{x}_{k-1} \quad \hat{x}_{k-1} + \sqrt{(L+\lambda)(P_{k-1} + Q_{k-1})} \quad \hat{x}_{k-1} - \sqrt{(L+\lambda)(P_{k-1} + Q_{k-1})}] \tag{10}$$

L is the dimension of the state variable and $\lambda = \alpha^2(L + \kappa) - L$ is scaling parameter. α determines the spread of the sigma points around $\bar{x}$, the average value of sigma points, and is usually set to a small positive value (e.g.10^{-3}). κ is a secondary scaling parameter which is usually set to 0.

The transformed sigma points are propagated through the nonlinear function f. The predicted state vector $\hat{x}_k^-$ and predicted state covariance matrix P_k^- are computed using a weighted sample mean and covariance of the posterior sigma points with corresponding weights W_i. β is used to incorporate prior knowledge of the distribution of x. It is set as $\beta = 2$ for Gaussian distribution [4].

$$X_{i,k} = f(X_{i,k-1}, u_{k-1}) \tag{11}$$
$$\hat{x}_k^- = \sum_{i=0}^{2L} W_i^{(m)} X_{i,k} \tag{12}$$
$$P_k^- = \sum_{i=0}^{2L} W_i^{(c)} \{X_{i,k} - \hat{x}_k^-\}\{X_{i,k} - \hat{x}_k^-\}^T \tag{13}$$
$$W_0^{(m)} = \frac{\lambda}{(L+\lambda)} \quad W_0^{(c)} = \frac{\lambda}{(L+\lambda)} + (1 - \alpha^2 + \beta) \tag{14}$$
$$W_i^{(m)} = W_i^{(c)} = \frac{1}{2(L+\lambda)} \quad i = 1, 2, \ldots, 2L \tag{15}$$

The predicted observation vector $\hat{y}_k^-$ and the predicted output covariance matrix P_k^{yy} is calculated using nonlinear observation function h.

$$Y_{i,k} = h(X_{i,k}) \tag{16}$$
$$\hat{y}_k^- = \sum_{i=0}^{2L} W_i^{(m)} Y_{i,k} \tag{17}$$
$$P_k^{yy} = \sum_{i=0}^{2L} W_i^{(c)} \{Y_{i,k} - \hat{y}_k^-\}\{Y_{i,k} - \hat{y}_k^-\}^T \tag{18}$$

With the innovation covariance matrix P_k^{vv} and the cross-correlation matrix P_k^{xy}, the Kalman filter gain K_k is computed as follows

$$P_k^{vv} = P_k^{yy} + R_k \tag{19}$$
$$P_k^{xy} = \sum_{i=0}^{2L} W_i^{(c)} \{X_{i,k} - \hat{x}_k^-\}\{Y_{i,k} - \hat{y}_k^-\}^T \tag{20}$$
$$K_k = P_k^{xy} (P_k^{vv})^{-1} \tag{21}$$

When GPS data is given, the state vector and state covariance matrix are updated.

$$\hat{x}_k = \hat{x}_k^- + K_k(y_k - \hat{y}_k^-) \tag{22}$$
$$P_k = P_k^- - K_k P_k^{vv} K_k^T \tag{23}$$

3. OBSERVABILITY ANALYSIS

In this section, we provide an observability analysis of the GPS-IMU system. We first construct a system error dynamics equation in section 3.1 and then analyze it for the time invariant case in section 3.2. Extending the result of 3.2, a consideration for the time variant case will be given in section 3.3. We note that the contents of section 3.1∼3.3 are mainly a replication of the work in [8]. Then in section 3.4, we provide an identification of an important subset of the unobservable motion, namely

constant attitude with linear acceleration, constant attitude with quadratic acceleration, and constant speed orbital motion. The analysis of the observability of orbital motion is given by [3], but we mention it here since we think they are an important special case.

3.1 Error Dynamics

In this section, we will neglect the gravity gradient and rotational motion of the earth. δP,δV,$\delta\psi$,δb_a, and δb_g indicate the perturbation of position, velocity, attitude angle, acceleration bias, and gyro bias. F is a specific force acting on the system and w_{eb} is an angular velocity of the body frame. Superscript e and b indicate the earth NED frame and body frame and C_B^E is the coordinate transformation matrix from the body frame to the NED frame. The linear perturbation equations and the measurement equation are described as

$$\begin{bmatrix} \delta\dot{P}^e \\ \delta\dot{V}^e \\ \delta\dot{\psi}^e \\ \delta\dot{b}_a^b \\ \delta\dot{b}_g^b \end{bmatrix} = \begin{bmatrix} 0 & I & 0 & 0 & 0 \\ 0 & 0 & -[C_B^E F^b]^\times & C_B^E & 0 \\ 0 & 0 & -[w_{eb}^b]^\times & 0 & C_B^E \\ 0 & 0 & 0 & 0 & 0 \\ 0 & 0 & 0 & 0 & 0 \end{bmatrix} \begin{bmatrix} \delta P^e \\ \delta V^e \\ \delta\psi^e \\ \delta b_a^b \\ \delta b_g^b \end{bmatrix} \tag{24}$$

$$z = \begin{bmatrix} I & 0 & 0 & 0 & 0 \\ 0 & I & 0 & 0 & 0 \end{bmatrix} \begin{bmatrix} \delta P^e \\ \delta V^e \\ \delta\psi^e \\ \delta b_a^b \\ \delta b_g^b \end{bmatrix} \tag{25}$$

Since the position error is measured directly, the observability of the system can be analyzed on the reduced system.

$$\begin{bmatrix} \delta\dot{V}^e \\ \delta\dot{\psi}^e \\ \delta\dot{b}_a^b \\ \delta\dot{b}_g^b \end{bmatrix} = \begin{bmatrix} 0 & -[C_B^E F^b]^\times & C_B^E & 0 \\ 0 & -[w_{eb}^b]^\times & 0 & C_B^E \\ 0 & 0 & 0 & 0 \\ 0 & 0 & 0 & 0 \end{bmatrix} \begin{bmatrix} \delta V^e \\ \delta\psi^e \\ \delta b_a^b \\ \delta b_g^b \end{bmatrix} \tag{26}$$

$$z = \begin{bmatrix} I & 0 & 0 & 0 \end{bmatrix} \begin{bmatrix} \delta V^e \\ \delta\psi^e \\ \delta b_a^b \\ \delta b_g^b \end{bmatrix} \tag{27}$$

3.2 Time-invariant System

A time-invariant system is when the specific force acting on the system is constant and the system is not experiencing rotation motion. We will use a transformed state vector $\bar{x}$ to analyze the time-invariant system.

$$\bar{x} = \begin{bmatrix} \delta V^e \\ \delta b_a^b - [F^b]^\times C_E^B \delta\psi^e \\ \delta b_g^b - [w_{eb}^b]^\times C_E^B \delta\psi^e \\ \delta\psi^e \end{bmatrix} \tag{28}$$

With this transformed state vector $\bar{x}$, system matrices change as

$$\bar{A} = \begin{bmatrix} 0 & C_B^E & 0 & 0 \\ 0 & 0 & -[F^b]^\times & 0 \\ 0 & 0 & -[w_{eb}^b]^\times & 0 \\ 0 & 0 & C_B^E & 0 \end{bmatrix} \tag{29}$$

$$\bar{H} = \begin{bmatrix} I & 0 & 0 & 0 \end{bmatrix} \tag{30}$$

We can find the zeros in the last column of $\bar{A}$ and $\bar{H}$. This is the advantage we have when we use transformed state vector $\bar{x}$. We can calculate the observability matrix as follows

$$O = \begin{bmatrix} \bar{H} \\ \bar{H}\bar{A} \\ \bar{H}\bar{A}^2 \\ \vdots \\ \bar{H}\bar{A}^k \\ \vdots \\ \bar{H}\bar{A}^{11} \end{bmatrix} = \begin{bmatrix} I & 0 & 0 & 0 \\ 0 & C_B^E & 0 & 0 \\ 0 & 0 & O_{2,3} & 0 \\ \vdots & \vdots & \vdots & \vdots \\ 0 & 0 & O_{k,3} & 0 \\ \vdots & \vdots & \vdots & \vdots \\ 0 & 0 & O_{11,3} & 0 \end{bmatrix} \tag{31}$$

where

$$O_{2,3} = -C_B^E [F^b]^\times \tag{32}$$

$$O_{k,3} = -O_{k-1,3}[w_{eb}^b]^\times \tag{33}$$

Based on this, observability analysis of time-invariant systems can be divided into 2 cases.

1) If $F^b = 0$ and $w_{eb}^b = 0$, system has 6 unobservable modes. Attitude error and gyro bias are unobservable in this condition. However, this case happens only when the system is experiencing free-fall.

2) If $F^b \neq 0$ and $w_{eb}^b = 0$, system has 4 unobservable modes. An additional unobservable mode is $\bar{x} = [0\,0\,F^b\,0]^T$. This means that the gyro bias in the direction of the specific force is unobservable. An example of this motion is constant acceleration and attitude motion.

3.3 Time-variant System

In section 3.2, we introduced a state transformation $x = T\bar{x}$. We use the same transformation to analyze the time-variant system. i.e.,

$$T = \begin{bmatrix} I & 0 & 0 & 0 \\ 0 & 0 & 0 & I \\ 0 & I & 0 & T_f \\ 0 & 0 & 0 & T_w \end{bmatrix} \tag{34}$$

$$T_f = [F^b]^\times C_E^B \quad T_w = -C_E^B [w_{eb}^b]^\times \tag{35}$$

$$x = T\bar{x} \tag{36}$$

The transformed system is given as

$$\dot{\bar{x}} = T^{-1}(AT + \dot{T})\bar{x} = \bar{A}\bar{x} \tag{37}$$

$$z = HT\bar{x} = \bar{H}\bar{x} \tag{38}$$

Therefore,

$$\bar{A} = \begin{bmatrix} 0 & C_B^E & 0 & 0 \\ 0 & 0 & -[F^b]^\times & \dot{T}_f \\ 0 & 0 & -[w_{eb}^b]^\times & \dot{T}_w \\ 0 & 0 & C_B^E & 0 \end{bmatrix} \tag{39}$$

$$\bar{H} = \begin{bmatrix} I & 0 & 0 & 0 \end{bmatrix} \tag{40}$$

$$\dot{T}_f = ([\dot{F}^b]^\times - [F^b]^\times [w_{eb}^b]^\times) C_E^B \tag{41}$$

$$\dot{T}_w = [w_{eb}^b]^\times C_E^B [w_{eb}^b]^\times \tag{42}$$

Observability matrix of the transformed time-varying system is constructed as

$$O(t) = \begin{bmatrix} I & 0 & 0 & 0 \\ 0 & C_B^E & 0 & 0 \\ 0 & O_{2,2} & O_{2,3} & O_{2,4} \\ \vdots & \vdots & \vdots & \vdots \\ 0 & O_{k,2} & O_{k,3} & O_{k,4} \\ \vdots & \vdots & \vdots & \vdots \\ 0 & O_{11,2} & O_{11,3} & O_{11,4} \end{bmatrix} \tag{43}$$

for $k = 2, 3, \ldots, 11$

$$O_{k,2} = \dot{O}_{k-1,2} \tag{44}$$

$$O_{k,3} = -O_{k-1,2}[F^b]^\times - O_{k-1,3}[w_{eb}^b]^\times + O_{k-1,4} C_B^E + \dot{O}_{k-1,3} \tag{45}$$

$$O_{k,4} = O_{k-1,2}\dot{T}_f + O_{k-1,3}\dot{T}_w + \dot{O}_{k-1,4} \tag{46}$$

Since C_B^E has rank 3, the observability of the system depends on the rank of O_{sub}

$$O_{\text{sub}} = \begin{bmatrix} O_{2,3} & O_{2,4} \\ \vdots & \vdots \\ O_{k,3} & O_{k,4} \\ \vdots & \vdots \\ O_{11,3} & O_{11,4} \end{bmatrix} \tag{47}$$

3.4 Low Observability Motion

With the observability matrix above, the number of unobservable states in various motions can be calculated. For instance, as shown by [3], constant speed orbital motion has three dimensional unobservable space. In this section, we provide further identification of unobservable motions, focusing on a constant attitude case.

Constant velocity motion and constant acceleration motion is a typical example of the time-invariant system with constant attitude. These systems have 4 unobservable modes as shown in section 3.2. However, in the time-varying system, which has the angular velocity or the change of specific force, the rank of O_{sub} should be calculated to obtain the unobservable mode.

Using $\dot{C}_B^E = 0$ and $w_{eb}^b = 0$ of constant attitude motion, O_{sub} reduces as follows

$$O_{2,3} = -[F^e]^\times C_B^E \tag{48}$$

$$O_{2,4} = [\dot{F}^e]^\times \tag{49}$$

$$O_{k,3} = O_{k-1,4} C_B^E + \dot{O}_{k-1,3} \tag{50}$$

$$O_{k,4} = \dot{O}_{k-1,4} \tag{51}$$

We calculated the first three row elements for example

$$O_{2,3} = -[F^e]^\times C_B^E \qquad O_{2,4} = [\dot{F}^e]^\times \tag{52}$$

$$O_{3,3} = 0 \qquad O_{3,4} = [\ddot{F}^e]^\times \tag{53}$$

$$O_{4,3} = [\ddot{F}^e]^\times C_B^E \qquad O_{4,4} = [\dddot{F}^e]^\times \tag{54}$$

The number of unobservable modes in the time-variant system is given in Table 1. The proof for the constant attitude motion is given below.

Table 1. Examples of low observability motion in time-varying system.

	Description	Unobservable modes
(1)	Linear acceleration	2
(2)	Ascending with quadratical acceleration	2
(3)	Orbit motion	3

Proof:

1) In linear acceleration,

$$O_{2,3} = -[F^e]^\times C_B^E \qquad O_{2,4} = [\dot{F}^e]^\times \tag{55}$$

$$O_{k,3} = 0 \qquad O_{k,4} = 0 \tag{56}$$

The nullspace of O_{sub} is $[F^e \;\; 0]$ and $[0 \;\; \dot{F}^e]$. With this nullspace, we can find that the gyro bias in the direction of specific force and attitude error in the direction of $\dot{F}^e$ is unobservable.

2) In ascending motion with quadratic acceleration,

$$O_{2,3} = -[F^e]^\times C_B^E \qquad O_{2,4} = [\dot{F}^e]^\times \tag{57}$$

$$O_{3,3} = 0 \qquad O_{3,4} = [\ddot{F}^e]^\times \tag{58}$$

$$O_{4,3} = [\ddot{F}^e]^\times C_B^E \qquad O_{4,4} = 0 \tag{59}$$

$$O_{k,3} = 0 \qquad O_{k,4} = 0 \tag{60}$$

However, $O_{2,3} = -[F^e]^\times C_B^E$ and $O_{4,3} = [\ddot{F^e}]^\times C_B^E$ has the same nullspace because F^e and $\ddot{F}^e$ is linearly dependent. Similarly, $O_{2,4}$ and $O_{3,4}$ have the same nullspace. Therefore, the rank of $O_{\text{sub}} = 4$. Unobservable mode is gyro bias and attitude error in the direction of earth gravity.

■

For the proof of orbit motion observability analysis, refer to [3].

4. BOUNDARY CASE PERFORMANCE COMPARISON OF EKF AND UKF

Numerical Simulations are given in 9 conditions. Table 3 gives the descriptions and the number of unobserv-

Table 2. Simulation results.

	EKF				UKF			
	Hor(m)	Ver(m)	Pos(m)	Att(rad)	Hor(m)	Ver(m)	Pos(m)	Att(rad)
1	4.6919	11.3245	12.9926	0.5724	2.9943	3.7001	5.1377	0.0335
2	6.0579	11.6537	14.4214	1.0692	4.29624	3.1355	5.8471	0.0802
3	4.9017	14.4913	16.003	0.7118	2.9918	4.5183	5.8437	0.0337
4	5.5010	12.5891	14.8623	0.8666	3.7457	4.0752	6.1851	0.0988
5	5.1385	12.2204	14.0525	1.0814	3.1916	4.5457	6.0099	0.0309
6	4.8537	12.8603	14.5230	0.8986	2.8368	3.5145	4.9031	0.0457
7	5.8088	11.6579	14.1556	1.4103	4.0715	5.6063	6.8863	0.3548
8	4.8417	12.3995	14.0129	0.5492	4.0564	4.1967	6.2285	0.0338
9	5.0777	11.8818	13.6924	0.5693	3.1794	4.4784	6.0868	0.1078

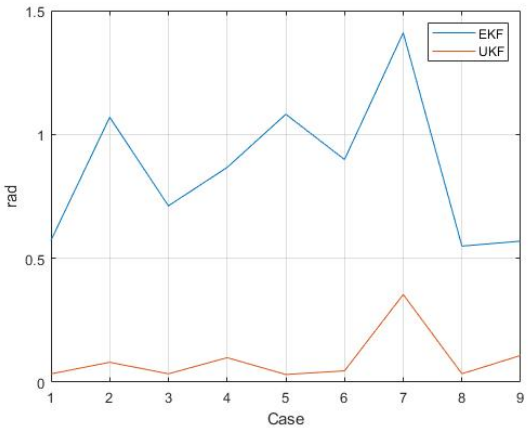

Fig. 1. Simulation attitude error.

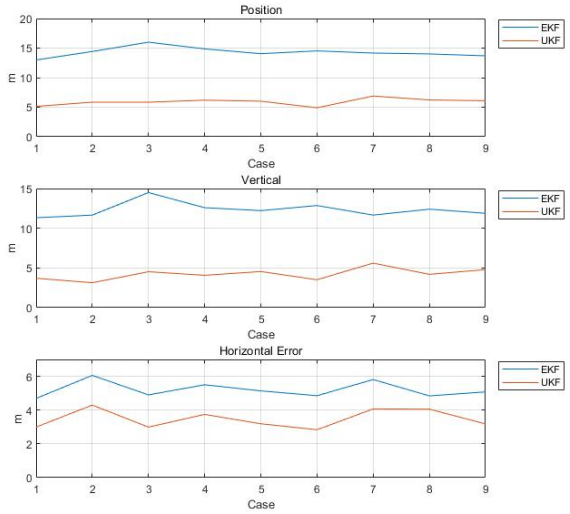

Fig. 2. Simulation position error.

able modes of the maneuvers. Maneuver (8)∼(9) are reference maneuvers in which both the acceleration and attitude change, therefore, do not have any unobservable mode.

Total 30 datasets are created and saved for each maneuver and the average of Mean-Square-Error is calculated. To exclude the effect of the Gaussian noise and

Table 3. Simulated motions.

	Description	Unobservable modes
(1)	Hovering	4
(2)	Constant-speed in xy plane	4
(3)	Constant Acceleration in xy plane	4
(4)	x:constant speed y:constant acceleration	4
(5)	Linear acceleration	2
(6)	Ascending with quadratical acceleration	2
(7)	Orbit motion	3
(8)	x:linearly increasing acceleration y:quadratically increasing acceleration	0
(9)	Rotation in xy plane with constant angular acceleration	0

random walk of IMU and GPS, each EKF and UKF simulations are conducted on the same dataset. In the artificial dataset setting, GPS horizontal accuracy and vertical accuracy are set to 5m and 20m each. Mean-Square-Error of each maneuver is given in the figure. Attitude error is the size of the rotation vector.

5. CONCLUSION

We investigated the performance difference of EKF and UKF on GPS-IMU-based UAV localization in low-observability motions. While UKF requires more implementation effort than EKF, UKF showed a better performance in position and attitude estimation than EKF. Its performance difference in attitude estimation was significant. Considering that the attitude error difference between EKF and UKF slightly dropped in the reference observable motion (8)∼(9), this attitude estimation dif-

ference can be suspected to the result of large nonlinearity due to gyro bias and attitude error unobservability. When the nonlinearity of the system gets larger, the performance gap between EKF and UKF would increase since EKF only approximates first-order terms while UKF captures accurately to the 3rd order.

Also, it is noticeable that vertical error and attitude error of the EKF and UKF showed a large gap in the low observability condition while horizontal error in the same condition was in the same order. The vertical error of the UKF was around 5m. Considering the large vertical error of the GPS signal, it might be effective to consider the UKF algorithm to reduce the vertical error.

ACKNOWLEDGEMENT

This research was supported by a grant to Bio-Mimetic Robot Research Center Funded by Defense Acquisition Program Administration, and by Agency for Defense Development (UD190018ID).

REFERENCES

[1] Y. Lee, J. Yoon, H. Yang, C. Kim, and D. Lee, "Camera-gps-imu sensor fusion for autonomous flying," in *2016 Eighth International Conference on Ubiquitous and Future Networks (ICUFN)*, pp. 85–88, IEEE, 2016.

[2] D. Chen and G. X. Gao, "Probabilistic graphical fusion of lidar, gps, and 3d building maps for urban uav navigation," *NAVIGATION, Journal of the Institute of Navigation*, vol. 66, no. 1, pp. 151–168, 2019.

[3] S. Hong, M. H. Lee, H.-H. Chun, S.-H. Kwon, and J. L. Speyer, "Observability of error states in gps/ins integration," *IEEE Transactions on Vehicular Technology*, vol. 54, no. 2, pp. 731–743, 2005.

[4] E. A. Wan and R. Van Der Merwe, "The unscented kalman filter for nonlinear estimation," in *Proceedings of the IEEE 2000 Adaptive Systems for Signal Processing, Communications, and Control Symposium (Cat. No. 00EX373)*, pp. 153–158, Ieee, 2000.

[5] B. Allotta, L. Chisci, R. Costanzi, F. Fanelli, C. Fantacci, E. Meli, A. Ridolfi, A. Caiti, F. Di Corato, and D. Fenucci, "A comparison between ekf-based and ukf-based navigation algorithms for auvs localization," in *OCEANS 2015-Genova*, pp. 1–5, IEEE, 2015.

[6] J. Gross, Y. Gu, S. Gururajan, B. Seanor, and M. Napolitano, "A comparison of extended kalman filter, sigma-point kalman filter, and particle filter in gps/ins sensor fusion," in *AIAA guidance, navigation, and control conference*, p. 8332, 2010.

[7] M. Rhudy, Y. Gu, J. Gross, and M. Napolitano, "Sensitivity analysis of ekf and ukf in gps/ins sensor fusion," in *AIAA guidance, navigation, and control conference*, p. 6491, 2011.

[8] I. Rhee, M. F. Abdel-Hafez, and J. L. Speyer, "Observability of an integrated gps/ins during maneuvers," *IEEE Transactions on Aerospace and Electronic systems*, vol. 40, no. 2, pp. 526–535, 2004.